4-29-2016

Inflationary Gravitational Waves and B-Mode Polarization of the Cosmic Microwave Background

Kiley Todd Heflin

Inflationary Gravitational Waves and B-Mode Polarization of the Cosmic Microwave Background

by

Kiley Todd Heflin

An Honors Capstone
submitted in partial fulfillment of the requirements
for the Honors Diploma
to

The Honors College

of

The University of Alabama in Huntsville

4/29/16

Honors Capstone Director: Dr. Richard Lieu
Distinguished Professor of Physics

Kiley Heflin — May 2nd, 2016
Student — Date

Richard Lieu — 2nd May, 2016
Director — Date

[signature] — May 2, 2016
Department Chair — Date

[signature] — 5/9/16
Honors College Dean — Date

HONORS COLLEGE
THE UNIVERSITY OF ALABAMA IN HUNTSVILLE

Honors College
Frank Franz Hall
+1 (256) 824-6450 (voice)
+1 (256) 824-7339 (fax)
honors@uah.edu

Honors Thesis Copyright Permission

This form must be signed by the student and submitted as a bound part of the thesis.

In presenting this thesis in partial fulfillment of the requirements for Honors Diploma or Certificate from The University of Alabama in Huntsville, I agree that the Library of this University shall make it freely available for inspection. I further agree that permission for extensive copying for scholarly purposes may be granted by my advisor or, in his/her absence, by the Chair of the Department, Director of the Program, or the Dean of the Honors College. It is also understood that due recognition shall be given to me and to The University of Alabama in Huntsville in any scholarly use which may be made of any material in this thesis.

Kiley Heflin
Student Name (printed)

Kiley Heflin
Student Signature

May 2nd, 2016
Date

TABLE OF CONTENTS

ABSTRACT

This paper is an attempt to introduce the concept of gravitational waves, interpret the results of BICEP2 and *Planck*, analyze the methods employed by both missions, and evaluate the implications of the existence of inflationary gravitational waves (IGWs). BICEP2/*Keck Array* are experiments aimed at measuring the polarization of the cosmic microwave background (CMB), as well as providing speculation regarding the origin of B-Mode polarization of the CMB. In June 2014, BICEP2 reported the detection of such polarization but acknowledged uncertainty regarding its origin due to the possibility of gravitational lensing caused by cosmic dust. BICEP2's detection used a CMB polarimeter specifically designed to observe the B-mode power spectrum around a multipole moment $\ell \sim 80$. In May 2015, the European Space Agency's *Planck* mission published a mapping of the intensity and polarization of the sky at microwave frequencies in an attempt to address the problem of cosmic dust. In a joint analysis of their data in 2015, BICEP2/*Keck Array* and *Planck*, by evaluating the tensor-to-scalar ratio *r*, concluded that confirmation of inflationary gravitational waves would require additional data. The detection of inflationary gravitational waves would have a profound impact on cosmology, and could provide insight into the earliest moments ($\sim 10^{-32}$s) after the Big Bang. The presence of IGWs, or lack thereof, may disconfirm or confirm, respectively, the validity of the standard ΛCDM-model of cosmology, which does not include a period of inflation.

INTRODUCTION

Gravitational Waves

Mass in nonspherical, nonuniform motion produces ripples in the curvature of spacetime referred to as gravitational waves. It is believed that gravitational waves are produced by a variety of astrophysical phenomena, including binary star systems, supernova explosions, collapse of black holes, and, as we shall explore, the big bang. For the sake of simplicity, this introduction will concern itself primarily with *linearized* gravitational waves. That is, a gravitational wave traveling through a flat spacetime (referred to here as Minkowski spacetime), denoted by the metric $g_{\alpha\beta}(x) = \eta_{\alpha\beta}$, where

$$\eta_{\alpha\beta} = \begin{array}{c} \\ t \\ x \\ y \\ z \end{array} \begin{array}{c} \begin{array}{cccc} t & x & y & z \end{array} \\ \begin{pmatrix} -1 & 0 & 0 & 0 \\ 0 & 1 & 0 & 0 \\ 0 & 0 & 1 & 0 \\ 0 & 0 & 0 & 1 \end{pmatrix} \end{array}.$$

Note that here we employ geometrized units (c = G = 1). Some properties of linearized gravitational waves are that they propagate at the speed of light, they are transverse, they have two independent polarizations, they can be detected by their effect on the relative motion of test masses, and they carry energy [15].

The propagation of a gravitational wave can be thought of in terms of a perturbing metric to the metric of Minkowski spacetime. Namely,

$$h_{\alpha\beta}(t, z) = \begin{array}{c} \\ t \\ x \\ y \\ z \end{array} \begin{array}{c} \begin{array}{cccc} t & x & y & z \end{array} \\ \begin{pmatrix} 0 & 0 & 0 & 0 \\ 0 & f_+(t-z) & f_\times(t-z) & 0 \\ 0 & f_\times(t-z) & -f_+(t-z) & 0 \\ 0 & 0 & 0 & 0 \end{pmatrix} \end{array}$$

where $f_{\times}(t - z)$ and $f_{+}(t - z)$ are representative of the two possible polarizations of our linearized gravitational wave traveling in the z-direction. Now, a complete description of our metric $g_{\alpha\beta}$ is available [15]:

$$g_{\alpha\beta}(t, z) = \eta_{\alpha\beta} + h_{\alpha\beta}(t, z).$$

For now, we need only consider the case of a gravitational wave of + (plus) polarization. In this case, our perturbing metric can be written

$$h_{\alpha\beta}(t, z) = \begin{array}{c} \\ t \\ x \\ y \\ z \end{array} \begin{array}{c} \begin{array}{cccc} t & x & y & z \end{array} \\ \begin{pmatrix} 0 & 0 & 0 & 0 \\ 0 & 1 & 0 & 0 \\ 0 & 0 & -1 & 0 \\ 0 & 0 & 0 & 0 \end{pmatrix} \end{array} f(t - z),$$

with $f(t - z)$ being any function of $t - z$ where $|f(t - z)| << 1$ (meaning that the perturbation is small) [15].

If we set $f(t - z) = a \sin[\omega(t - z)]$, we obtain an equation representative of a gravitational wave with frequency ω and amplitude a. Arranging a group of particles in a circle through the x-y plane around a central test mass with coordinates $(t, 0, 0, 0)$, we can see that directions perpendicular to the direction of propagation oscillate between a compressed state and an expanded state throughout time. The line element of such a spacetime is

$$ds^2 = -dt^2 + \{1 + a \sin[\omega(t - z)]\}dx^2 + \{1 - a \sin[\omega(t - z)]\}dy^2 + dz^2.$$

The line element illustrates the curvature of spacetime due to the gravitational wave, and corresponds to our metric, $g_{\alpha\beta}(t, z)$. We can see that as time increases, the actual distance

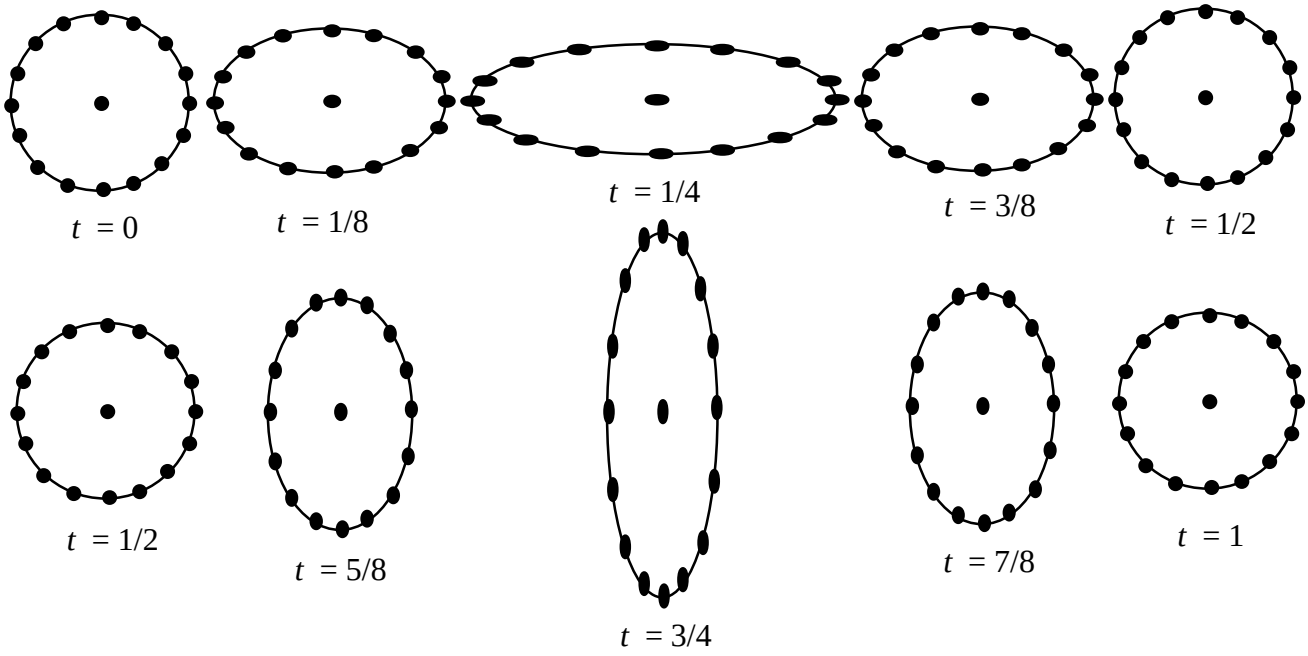

Figure 1: Compression and expansion of a ring of particles through time due to a gravitational wave propagating into the page, where the time *t* is measured in fractions of complete cycles (*t* = ½ indicates half a cycle).

between two points on the *x*-*y* plane oscillates. This becomes even more apparent if we define a new time-dependent coordinate system for the *x*-*y* plane:

$$X(t) = [1 + a \sin(\omega t)]x,$$

$$Y(t) = [1 + a \sin(\omega t)]y,$$

for which we receive the familiar Euclidean line element $dS^2 = dX^2 + dY^2$ [15]. This oscillation in the curvature of spacetime is responsible for the detection of B-modes in the CMB [19, 20, 23, 29, 30].

Polarization of Electromagnetic Radiation by Gravitational Waves

The CMB is characterized entirely by its temperature and polarization in a given direction. Gravitational waves have the potential to impart a unique polarization, called B-mode polarization, on radiation. As we will discover later, the presence of B-mode polarization in the CMB is a source of intrigue in cosmology, and can be indicative of IGWs. Before discussing the mathematics of E- and B-mode polarization, we shall explore them conceptually [19, 20, 23, 29, 30].

Consider an electron at rest in the midst of a pressure wave (Figure 2). From the reference point of the electron, a fluctuation in density occurs. Because density is a scalar, we refer to this as a scalar fluctuation. Next, consider the possibility of photons approaching the electron from all directions. Because there are fewer surfaces for them to scatter from, photons will, on average, prefer to scatter into regions of lower density (or higher temperature). An observer looking at this scenario would find that light is polarized in a horizontal direction for the moments in which the electron was in a cold region of a pressure wave propagating in the horizontal direction (Figure 2A). Conversely, an electron in a hot region of the same pressure wave will polarize light vertically (Figure 2B). The resulting polarization pattern is referred to as E-mode polarization and can be seen in Figure 3A [5].

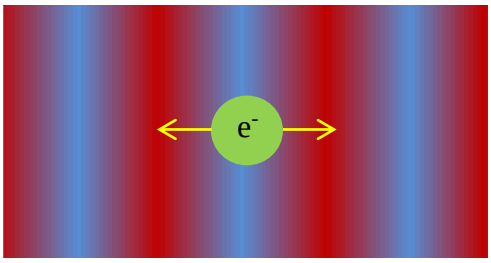

Figure 2A: Light polarizes horizontally when scattered off of an electron in a cold region of a pressure wave traveling in the *x*-direction.

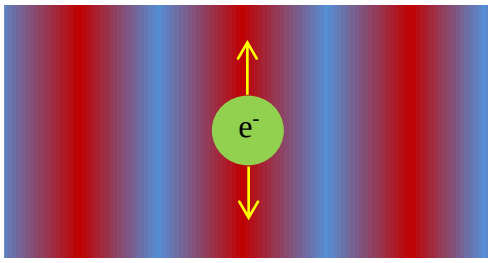

Figure 2B: Light polarizes vertically when scattered off of an electron in a hot region of a pressure wave traveling in the *x*-direction.

E-mode polarization can be produced by gravitational waves of plus (+) polarization as well as by pressure waves [5, 15]. Indeed, as is indicated by Figure 1, the effect of curved spacetime due to a + polarized gravitational wave propagating into the ring of particles is strikingly similar to the effect of a pressure wave propagating from left to right across the ring. If the central test mass is an electron, then t = ¾ in Figure 1 roughly corresponds to Figure 2A, where the electron is in a cold region of a pressure wave. Conversely, t = ¼ roughly corresponds to Figure 2B, where the electron is in a hot region of a pressure wave. This behavior is characteristic of dipoles, which can polarize in two directions (horizontal and vertical for our pressure wave). [5, 12, 13, 15]

This, of course, is but one of two possible polarizations of the gravitational wave. Consider the perturbing metric describing a cross (×) polarized gravitational wave:

$$h_{\alpha\beta}(t, z) = \begin{array}{c} \\ t \\ x \\ y \\ z \end{array} \begin{array}{c} \begin{array}{cccc} t & x & y & z \end{array} \\ \begin{pmatrix} 0 & 0 & 0 & 0 \\ 0 & 0 & 1 & 0 \\ 0 & 1 & 0 & 0 \\ 0 & 0 & 0 & 0 \end{pmatrix} \end{array} f(t - z).$$

Again, we'll suppose that $f(t - z) = a \sin[\omega(t - z)]$. In this case, the direction of oscillation of thering of particles is not vertical and horizontal but rather in the two diagonal directions. This, in turn, produces polarization in the diagonal directions, called B-mode polarization, as illustrated by Figure 3B. The fact that this type of polarization changes when reflected is reminiscent of curl, while the E-modes presented before, with their reflective invariance, are reminiscent of divergence. [5, 15, 16, 32]

In fact, this is where the terms "E-mode" and "B-mode" originate. In electrodynamics, Maxwell's Equations state [13]:

$$\nabla \cdot \mathbf{E} = \frac{1}{\epsilon_0}\rho \qquad \nabla \cdot \mathbf{B} = 0$$

$$\nabla \times \mathbf{E} = -\frac{\partial \mathbf{B}}{\partial t} \qquad \nabla \times \mathbf{B} = \mu_0 \mathbf{J} + \mu_0 \epsilon_0 \frac{\partial \mathbf{E}}{\partial t}$$

In the case of electrostatics, however, the partial derivatives with respect to time yield zero, causing the curl of the electric field to vanish. The only terms of consequence, then, are the divergence of the electric field ($\nabla \cdot \mathbf{E}$) and the curl of the magnetic field ($\nabla \times \mathbf{B}$). For this reason, when considering polarizations, divergence is associated with the electric field (E-modes) and curl with the magnetic field (B-modes). The analogy of E-modes and B-modes in polarization to electrostatics goes no further than this [5, 16, 32].

The most important piece of information to take away from this is that scalar fluctuations like pressure waves tend to only produce E-mode polarization, while tensor fluctuations like gravitational waves produce both E-modes and B-modes [5, 16, 23]. Because of this, the tensor-to-scalar ratio *r* is of great interest in the study of the polarization of the CMB [2, 3, 4, 28]. In order to calculate this tensor-to-scalar ratio, we must first consider Stokes' parameters.

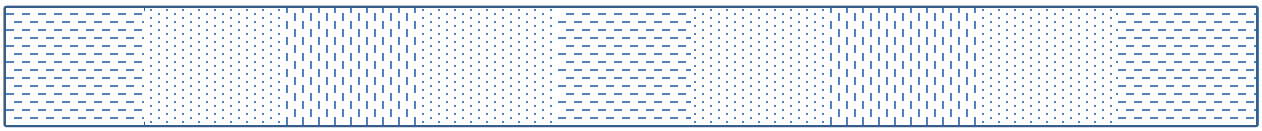

Figure 3A: E-mode polarization pattern. This pattern can be produced by both scalar and tensor fluctuations. Note that the areas between regions of vertical or horizontal polarization correspond to areas in between hot and cold regions of the density fluctuations in Figure 2.

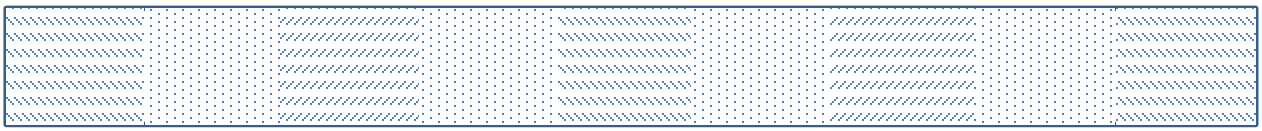

Figure 3B: B-mode polarization pattern. This pattern can only be produced by tensor fluctuations (as in gravitational waves). Note that, contrary to E-mode patterns, B-modes are not invariant under reflection. That is to say, if I were to hold Figure 3A up to a mirror, I would see the same image. If I were to hold Figure 3B up to a mirror, however, I would see a reflected image. Forward diagonal polarizations (/) would become backward diagonal polarizations (\ ). This characteristic is vital to understanding B-modes.

Polarization is characterized by the Stokes parameters *Q*, *U*, and *V*. For a monochromatic electromagnetic wave moving in the *z*-direction, the components of the wave's electric field vector are [19]

$$E_x = a_x(t)\cos[\omega_0 t - \theta_x(t)], \qquad E_y = a_y(t)\cos[\omega_0 t - \theta_y(t)]$$

where ω_0 represents frequency. The wave is considered polarized if these two components are correlated. The Stokes parameters are defined by the following relations [19, 20, 23, 27, 29, 30]:

$$I \equiv \langle a_x^2 \rangle + \langle a_y^2 \rangle,$$

$$Q \equiv \langle a_x^2 \rangle - \langle a_y^2 \rangle,$$

$$U \equiv \langle 2a_x a_y cos(\theta_x - \theta_y) \rangle,$$

$$V \equiv \langle 2a_x a_y sin(\theta_x - \theta_y) \rangle,$$

where the angled brackets denote time averages. Though the radiation intensity *I* does not directly characterize the polarization, it is sometimes necessary in the calculation of *Q* and *U*, which are used to determine E-mode and B-mode amplitudes. A complete description of polarization comes from the polarization tensor, given in spherical polar coordinates (θ, ϕ) as [19, 27]:

$$P_{ab}(\hat{\mathbf{n}}) = \frac{1}{2}\begin{pmatrix} Q(\hat{\mathbf{n}}) & -U(\hat{\mathbf{n}})sin\theta \\ -U(\hat{\mathbf{n}})sin\theta & -Q(\hat{\mathbf{n}})sin^2\theta \end{pmatrix}$$

The polarization tensor matrix is reminiscent of the *x*-*y* submatrix of the general form of the gravitational wave perturbation metric $h_{\alpha\beta}$ given earlier. Note that this similarity is not exact, since the polarization matrix is given in spherical polar coordinates, not Cartesian coordinates. As was suggested earlier, the plus mode of gravitational wave polarization is responsible for E-mode polarization of electromagnetic waves. Conversely, the cross mode of gravitational wave polarization is responsible for B-modes.

We seek to estimate power spectra relaying the amplitude of E-mode and B-mode polarization in the CMB as a function of multipole moment ℓ. Ref. [19] provides a complete derivation for such estimators. The result is:

$$\widehat{C_l^{\mathrm{G}}} = \sum_{m=-l}^{l} \frac{\left|a_{(lm)}^{\mathrm{G}}\right|^2}{2l+1}, \qquad \widehat{C_l^{\mathrm{C}}} = \sum_{m=-l}^{l} \frac{\left|a_{(lm)}^{\mathrm{C}}\right|^2}{2l+1},$$

where

$$a_{(lm)}^{\mathrm{G}} = \frac{1}{T_0}\int d\hat{\mathbf{n}} P_{ab}(\hat{\mathbf{n}}) Y_{(lm)}^{G\,ab*}(\hat{\mathbf{n}}), \qquad a_{(lm)}^{\mathrm{C}} = \frac{1}{T_0}\int d\hat{\mathbf{n}} P_{ab}(\hat{\mathbf{n}}) Y_{(lm)}^{C\,ab*}(\hat{\mathbf{n}}),$$

T_0 is the mean CMB temperature, and $Y_{(lm)}^{G\,ab}(\hat{\mathbf{n}})$ and $Y_{(lm)}^{C\,ab}(\hat{\mathbf{n}})$ are spherical harmonic functions [19, 20, 23, 29, 30]. The C_l^{G} and C_l^{C} estimators listed above provide approximations of power spectra corresponding to E-modes and B-modes, respectively, and an experimental calculation of these spectra was a primary goal for the BICEP2 mission.

It is worth noting that the propagation of a gravitational wave does not directly affect the polarization tensor. Rather, the gravitational wave alters the very metric of the polarization tensor according to the perturbing metric $h_{\alpha\beta}$. The metric of Minkowski spacetime in spherical polar coordinates is given by [15]:

$$\eta_{\alpha\beta} = \begin{array}{c} \\ t \\ r \\ \theta \\ \phi \end{array} \begin{array}{c} \begin{array}{cccc} t & r & \theta & \phi \end{array} \\ \begin{pmatrix} -1 & 0 & 0 & 0 \\ 0 & 1 & 0 & 0 \\ 0 & 0 & r^2 & 0 \\ 0 & 0 & 0 & r^2\sin^2\theta \end{pmatrix} \end{array}.$$

Alternatively, we can express this with the line element

$$ds^2 = -dt^2 + dr^2 + r^2 d\Omega^2,$$

where

$$d\Omega^2 = d\theta^2 + \sin^2\theta\, d\phi^2.$$

Our generalized metric is given, as before, by the formula

$$g_{\alpha\beta} = \eta_{\alpha\beta} + h_{\alpha\beta}.$$

We therefore require an expression for the perturbing metric $h_{\alpha\beta}$ of a gravitational wave propagating in the z-direction in spherical coordinates. Rewriting the metric listed earlier, we obtain

$$h_{\alpha\beta} = \begin{array}{c} \\ t \\ r \\ \theta \\ \phi \end{array} \begin{array}{c} \begin{array}{cccc} t & r & \theta & \phi \end{array} \\ \begin{pmatrix} 0 & 0 & 0 & 0 \\ 0 & f_+ sin\theta cos\phi + f_\times sin\theta sin\phi & f_\times sin\theta cos\phi - f_+ sin\theta sin\phi & 0 \\ 0 & f_+ cos\theta cos\phi + f_\times cos\theta sin\phi & f_\times cos\theta cos\phi - f_+ cos\theta sin\phi & 0 \\ 0 & -f_+ sin\phi + f_\times cos\phi & -f_\times sin\phi - f_+ cos\phi & 0 \end{pmatrix} \end{array}$$

via coordinate transformation. Our new metric $g_{\alpha\beta}$ differs from that of the Minkowski spacetime $\eta_{\alpha\beta}$ by this perturbation, and is given by:

$$g_{\alpha\beta} = \begin{array}{c} \\ t \\ r \\ \theta \\ \phi \end{array} \begin{array}{c} \begin{array}{cccc} t & r & \theta & \phi \end{array} \\ \begin{pmatrix} -1 & 0 & 0 & 0 \\ 0 & 1 + f_+ sin\theta cos\phi + f_\times sin\theta sin\phi & f_\times sin\theta cos\phi - f_+ sin\theta sin\phi & 0 \\ 0 & f_+ cos\theta cos\phi + f_\times cos\theta sin\phi & r^2 + f_\times cos\theta cos\phi - f_+ cos\theta sin\phi & 0 \\ 0 & -f_+ sin\phi + f_\times cos\phi & -f_\times sin\phi - f_+ cos\phi & r^2 sin^2\theta \end{pmatrix} \end{array}$$

That this alteration to the Minkowski spacetime will have an effect on the polarization tensor $P_{ab}(\hat{\mathbf{n}})$ is immediately apparent.

We have seen that gravitational waves can "bend" electromagnetic waves into a polarized state by warping the spacetime through which they propagate. However, gravitational waves are not the only source of spacetime curvature. In fact, according to general relativity, any massive body curves spacetime around it. For such delicate phenomena as the polarization of CMB radiation, it is necessary to consider even the minutest contributions. Indeed, the influence of even IGWs is rather small due to the attenuation that occurs across the distances involved in detecting CMB polarization [4, 19, 20, 23, 29, 30]. In seeking the amount of polarization of the

CMB due to IGWs, then, it becomes necessary to determine and exclude perturbations to the spacetime metric due to cosmic dust. Though the effect of a single dust particle is negligible, the cumulative lensing effect that occurs over the distances traveled by CMB radiation can have a profound effect on polarization. This lensing effect can produce B-modes from E-modes which are distinct from inflationary gravitational waves [4]. It is therefore imperative that some method be employed to rule out contributions due to cosmic dust.

Following BICEP2's declaration in June 2014 of the potential discovery of IGWs [3], this imperative fell on the European Space Agency's *Planck* mission. In May 2015, the *Planck* team published a mapping of the intensity and polarization of the sky at microwave frequencies in an attempt to address the problem of cosmic dust [28]. The data collected by *Planck* provided a framework for the members of both teams to evaluate dust contribution and attempt to either confirm or disconfirm, once and for all, the possibility of IGWs [4].

Inflationary Gravitational Waves in Cosmology

The verification of the existence or nonexistence of IGWs will shape the development of cosmology, and could potentially disprove the standard ΛCDM-model of cosmology, which does not include a period of inflation. Ref. [24] approximates the Friedmann equation, which governs the expansion of spacetime, as

$$|\Omega - 1| = \frac{|k|}{a^2 H^2}$$

with the density parameter Ω representing total energy density, the scale factor *a* representing the total size of the universe, *k* representing the spatial curvature of the universe, and Hubble parameter *H*. Typically, a^2H^2 is decreasing. This means that Ω strays from unity, given that Ω starts near one. In other words, $\Omega = 1$ is an unstable critical point. Based on current observations, Ω appears to be within an order of magnitude of one. The instability of this value under conventional big bang models coupled with the observational evidence for it necessitates a period during which the Hubble length

$$D = \frac{c}{H},$$

which is the distance from the observer at which objects appear to be moving away at the speed of light, was decreasing. That is to say,

$$\frac{d(c/H)}{dt} < 0.$$

This is the inflationary solution to the so-called flatness problem, and helps to explain isotropies in regions of the CMB that were not causally connected in the early universe. [6, 20, 21, 24]

This early period of inflation would involve significant perturbations to spacetime in the form of IGWs [15], detectable through B-mode polarization of the CMB [3, 4, 28]. Though these perturbations were initially very violent, their propagation since the inflationary period

would significantly decrease their amplitude, making them more difficult to detect directly [4]. The successful detection of an IGW, however, would provide conclusive evidence for an inflationary period in the history of our universe, and would significantly alter the pool of valid cosmological theories [6, 20, 21, 24]. In the next section, we will discuss the methods used in the BICEP2 and *Planck* missions in determining the validity of a potential IGW detection via measurement of B-mode polarization of the CMB.

METHODS AND INSTRUMENTS

The BICEP, or Background Imaging of Cosmic Extragalactic Polarization, and *Keck Array* experiment series began in January 2006 with BICEP1 [2, 17]. Due to the striking similarities between BICEP1 and BICEP2, we shall endeavor to explain the BICEP1 instrument before moving on to BICEP2. Known during its development as the Robinson Gravitational Wave Background Telescope, BICEP1 first began observing in the 100 – 220 GHz (1.2 – 3.0 mm) range from the Dark Sector Laboratory at the Amundsen-Scott South Pole station in order to exploit the exceptional ~1 mm wavelength transparency of the atmosphere above the cold Polar plateau. The BICEP1 receiver was comprised of a focal plane of 49 Polarization-Sensitive-Bolometer (PSB) pairs. A PSB is, essentially, a device which provides simultaneously a measurement of total intensity and the difference between orthogonal linear polarizations (Stokes *I* and *Q*, respectively). Though PSBs can operate at frequencies up to 600 GHz (0.5 mm), the BICEP1 device, for a majority of its operations, featured 25 PSB pairs at 100 GHz, 22 at 150 GHz, and two at 220 GHz. The PSBs were arranged in pairs such that each member of a pair would respond to orthogonal linear polarizations. A two-lens refracting telescope provided full width half-maximum (FWHM) angular resolution of 0.93° at 100 GHz and 0.60° at 150 GHz and an 18° field of view. [2, 3, 4, 17]

BICEP1 spent 85% of its total operating time focusing on a region known as the "Southern Hole" (located at a right ascension and declination range of $|\alpha| < 60°$ and $-70° < \delta < -45°$), which was selected due to its low dust emission (shown in Figures 4 and 5). The apparatus operated over a two-day cycle, with four nine-hour phases observing the Southern Hole. Each phase consisted of ten 50-minute long scansets, each comprised of 50 leftward and 50 rightward half-scans. Scanning at 0.25° steps in elevation between scansets, the telescope covered the full

CMB field after just two phases [2, 3]. We are, however, only concerned with BICEP1 to the extent that it is similar to BICEP2 (for more information on BICEP1, consult Ref. [2]).

Like BICEP1, the optical system of BICEP2 featured a 26.4 cm aperture all-cold refractor in a housing cooled by liquid helium. According to Ref. [3], BICEP2 differed from BICEP1 mainly in the use of a focal plane array of planar antenna-coupled devices with voltage-biased transition-edge sensor (TES) detectors and a multiplexed superconducting

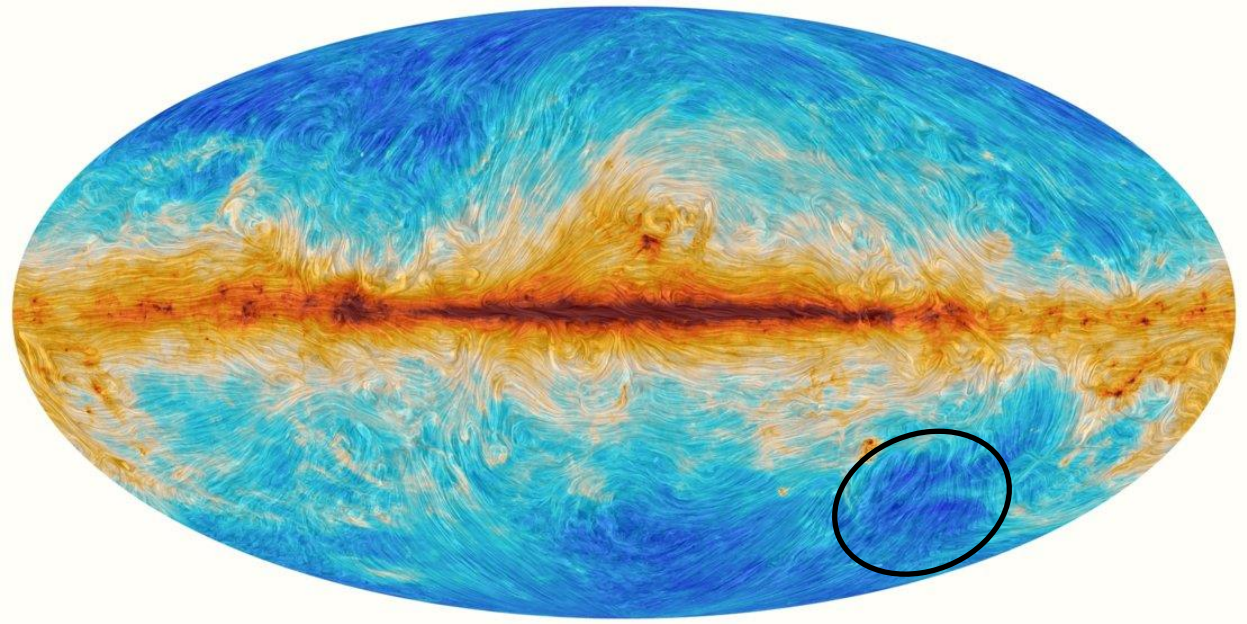

Figure 4: A map of polarized dust emissions released by the *Planck* collaboration. The circled region indicates the so called "Southern Hole", an area of minimal polarized dust emissions. This has been an area of primary focus in studying the polarization of the CMB. [11]

quantum interference device (SQUID) readout. A TES is a superconducting detector designed to detect individual photons. When a photon strikes the tiny superconducting circuit, its energy is absorbed as heat. The rise in temperature causes a slight increase in electrical resistance and a slight decrease in current, which is registered in the electronics of the unit as the detection of a photon. SQUIDs are very sensitive detectors of magnetic flux typically fabricated from thin films of niobium or of $YBa_2Cu_3O_7$. SQUIDs are often used to measure a variety of physical quantities, including magnetic field, magnetic field gradient, voltage, and magnetic susceptibility. [2, 3, 22, 26, 31]

As in BICEP1, the BICEP2 mission operated in 50 minute scansets. During this time, the telescope covered a 60° angle of fixed elevation, scanning 53 leftward and 53 rightward half-scans at 2.8° per second. Contrary to BICEP1, BICEP2 observed at only 150 GHz (2mm). The scan speed and angular resolution of the BICEP2 instrument formed a mapping of multipole ℓ = 100. Once again, BICEP2 primarily focused on imaging the Southern Hole due to the low contributions of cosmic dust to polarization measurements. Speculation surrounding the significance of cosmic dust contributions in this region ultimately led to *Planck*'s development of a comprehensive map of cosmic dust polarizations. [2, 3, 4, 28]

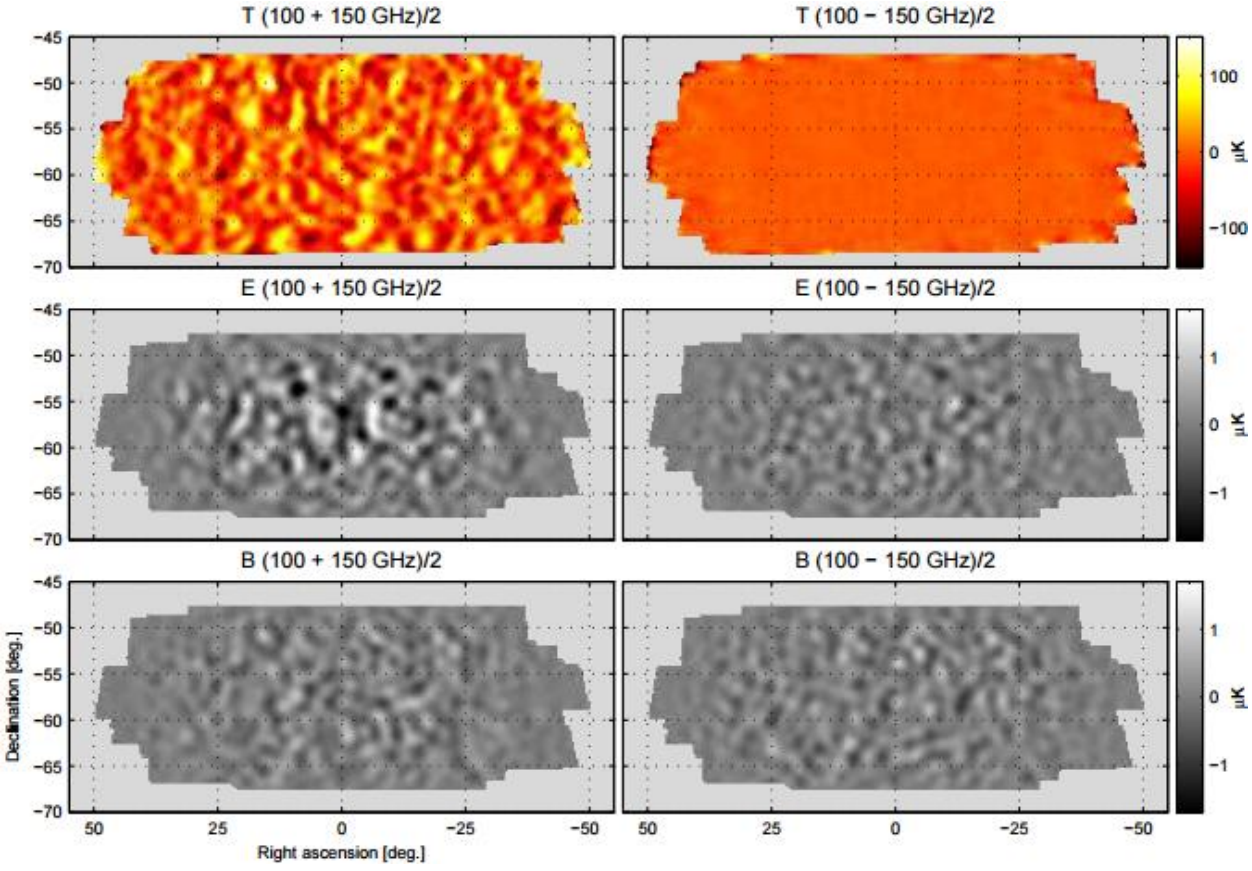

Figure 5: BICEP1's images of the Southern Hole. The images above were generated over three years of data collection. The top two images show temperature, the two images in the center display E-mode polarization, and the two images on the bottom display B-mode polarization. The left-side images show basic signal maps, and the right-side images show difference maps made from the first and second halves of the data set, produced by a method known as "jackknifing". As we shall see later, a similar approach to the one used to generate these images was repeated in the BICEP2 observations. [2]

The *Planck* spacecraft, launched in 2009, contained two major components: the payload and service modules. The payload module was made up of a telescope, cryogenic focal plane units of the Low Frequency Instrument (LFI) and the High Frequency Instrument (HFI), and the instrument cooling chains [8, 9]. The service module comprised a system for controlling power generation and management, devices for attitude and orbit monitoring and modification, ground-to-satellite data management systems, and radio frequency communications systems for data retrieval and command reception. The service module also stored elements of the instruments which did not require cooling as well as certain members of the cooling chains. Our primary focus will, obviously, be on the instruments aboard *Planck*. Of particular interest to us is the HFI, which addresses regions of the electromagnetic spectrum relevant to the studies of BICEP [9].

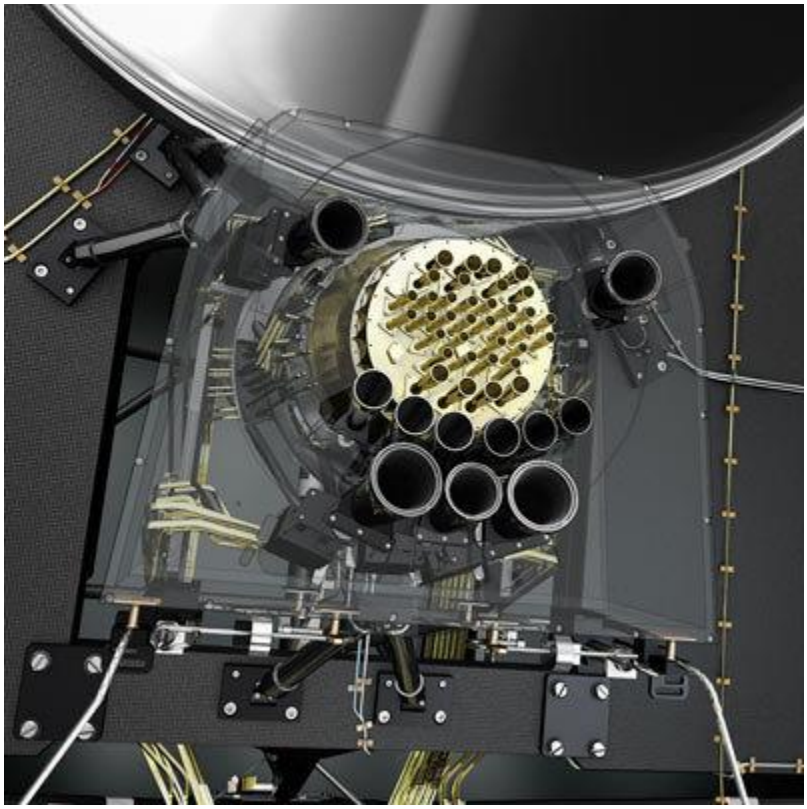

Figure 6: The combined focal plane of *Planck*'s two instruments. The HFI is the circle of horn-shaped wave guides at the center. The LFI is the outer ring of wave guides. These wave guides direct microwave radiation into the LFI and HFI. [7]

The LFI was designed to take measurements of the microwave sky in the 27 – 77 GHz (11.1 – 3.9 mm) range with high sensitivity [9]. The detector used by the LFI was a series of high electron mobility transistor (HEMT) radio receiver arrays. A HEMT is, essentially, a field-

effect transistor (FET) featuring a junction between two materials with different band gaps. For this reason, HEMTs are also known as heterostructure FETs (HFETs) or modulation-doped FETs (MODFETs). A material is said to be doped when impurities are introduced, reshaping the electron holes in the band structure of the material, thus forming a semiconductor. In the case of MODFETs, this doping effect is modulated by the formation of a junction between two materials. [12, 26]

The HFI was designed to take measurements of the microwave sky in the 84 GHz – 1 THz (3.6 – 0.3 mm) range with high sensitivity. The HFI featured a spider array of 52 bolometric detectors constructed from neutron transmutation doped (NTD) germanium thermistors. The use of NTD Ge thermistors is relatively common in the construction of large arrays like *Planck*'s HFI. This is due to the fact that NTD Ge thermometers tend to be quite uniform and also quite predictable. Germanium has four naturally occurring stable isotopes, two of which can produce a gallium-doped material. The isotopes are presumed to be distributed randomly throughout the resulting lattice. This, in turn, means that the neutron flux through large portions of the resulting NTD Ge is uniform. The uniformity of NTD Ge thermistors is due to the fact that multiple thermometers can be cut from relatively large blocks of NTD Ge. The thermistors constructed from NTD Ge are able to act as bolometric detectors due to the change in resistivity that occurs as heat is added to the system. This is registered in the electronics of the system in a manner reminiscent of the TES detectors mentioned before. [25]

The elements of both the HFI and the LFI were arranged in the focal plane (Figure 6) of a single telescope [7]. The telescope design featured on *Planck* was an off-axis tilted Gregorian system. The four classes of Gregorian telescopes are the classical Gregorian, the aplanatic Gregorian, and designs that either cancel out astigmatism or cancel out astigmatism and coma.

The Gregorian system featured on the *Planck* satellite belonged to the class which cancels out astigmatism. Such Gregorian telescopes are said to obey the Dragone-Mizuguchi condition, allowing them to operate without significant degradation over a large focal plane array. Submission to the Dragone-Mizuguchi condition also ensures that polarization of incoming electromagnetic radiation by the system itself is minimized [14]. This feature of the *Planck* satellite is obviously of critical importance to the study of polarized cosmic dust. The optical enclosure was formed from a large, self-supporting conical shield element covered with multi-layer insulation and was used to reduce the level of unwanted light produced by the spacecraft. In addition to this, the telescope featured a baffling element which shielded the HFI and LFI from thermal radiation originating from the optical enclosure [7].

Though the *Planck* mission ended in 2013, the wealth of data obtained from its observations continues to serve as an invaluable resource in the study of the CMB. The measurements made by the HFI and LFI were combined to produce an all-sky map (Figure 7) of CMB anisotropies, which is one of the richest sources of cosmological data to date. As we shall explore in the next section, data collected by the HFI was used to evaluate the extent to which B-mode polarization observed by BICEP2 was due to cosmic dust.

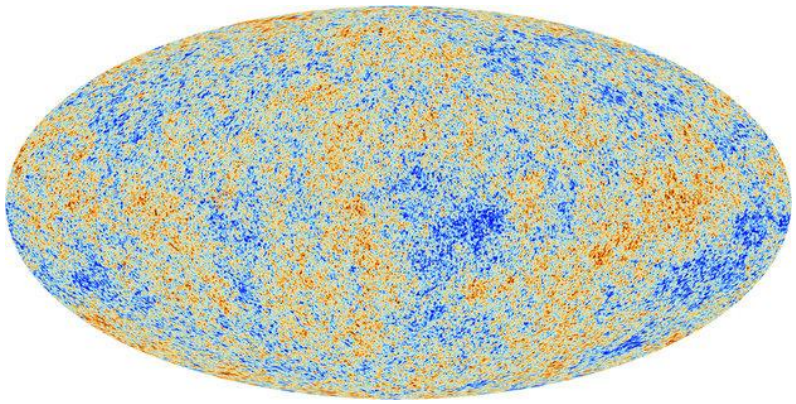

Figure 7: Map of cosmic microwave background anisotropies as observed by *Planck*. This image is based on the first 15 ½ months of observation by the *Planck* satellite. [10]

RESULTS

In their calculation of E-mode and B-mode power spectra, BICEP2 faced the issue of converting raw data in the form of Stokes *I* and *Q*. This was accomplished by constructing the amplitude of E-modes and B-modes from the Fourier Transform of Stokes *Q* and *U* (Stokes *U* can be derived from the raw data of Stokes *I* and *Q*). The means of these amplitudes squared were, in turn, taken as estimates of the CMB band powers. Further steps were taken to reduce the amount of E and B mixing that resulted from the implementation of this procedure. [3]

In the publication of their results, BICEP2 reported nine band powers, each approximately 35 multipoles wide, spanning the range $20 < \ell < 340$. After obtaining the sets of E and B Fourier modes, it became possible to form apodized E and B maps (Figure 8), which are reminiscent of the polarization patterns seen in Figure 3. These maps serve as another useful illustration of the characteristics of E and B modes. In the E signal maps, one can see a curl-less pattern that is invariant under reflection. In the B signal maps, one can see a divergence-less pattern that changes fundamentally under reflection. [3, 4]

More important than the formation of these maps, however, was the development of the power spectra as a function of multipole moment. Observationally, multipole moment corresponds roughly to angular resolution. With this in mind, the BICEP2 team was able to fit a tensor-to-scalar ratio *r* to the observed B-mode power spectrum. Their result was a tensor-to-scalar ratio $r = 0.20^{+0.07}_{-0.05}$. Initially, BICEP2 interpreted this result as an IGW detection, disregarding the perceived insignificant contribution of B-mode polarization due to cosmic dust. Their interpretation was based on the fact that the $r = 0.20$ value best matched their results in the regions of lower multipoles, particularly in the $\ell = 80$ region. This multipole region corresponds to the predicted value of the so called “recombination bump”, which is the expected location of a

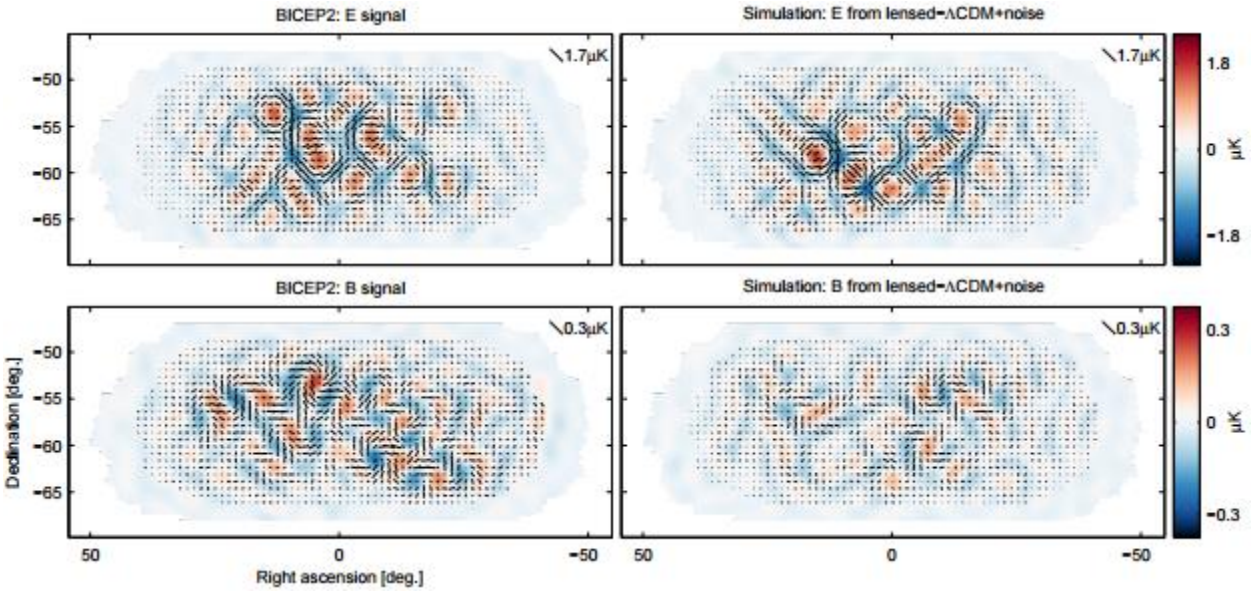

Figure 8: Maps of E and B modes obtained by BICEP2. The two images on the left represent actual data obtained by BICEP2. The two images on the right are obtained by simulations run by the BICEP2 team. [3]

peak in the IGW B-mode. (Another peak is predicted to exist at the $\ell < 10$ region, but measurement of this region is beyond the capabilities of the instruments discussed here.) [3, 4]

The BICEP2 team interpreted the $r = 0.20$ result to be an IGW detection based on the compatibility of a curve produced by such a value with the B-mode power spectrum at the multipole moment of the recombination bump [3]. Upon further analysis by the BICEP2 and *Planck* teams, however, at least some portion of this tensor-to-scalar ratio was due to gravitational lensing by cosmic dust. The result obtained by this join analysis was a cosmic dust tensor-to-scalar ratio of $r = 0.075$, meaning that approximately 38% of the tensor perturbations included in BICEP2's alleged IGW was due to cosmic dust [4].

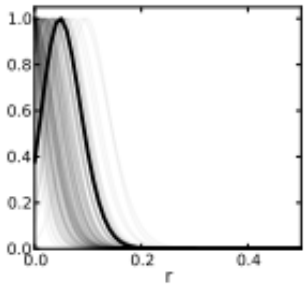

Figure 9: Likelihood of *r* as determined by the BICEP2/*Keck* and *Planck* joint analysis, using data from each team. Note the uncertainty in the result, with half of the curves peaking at $r = 0$. This is a useful illustration for the implicit uncertainty of the alleged IGW detection. [4]

CONCLUSION

The detection of IGWs is of critical importance to the confirmation of an inflationary period in the history of the universe, which in turn will provide a more accurate model of the evolution of the universe. IGWs can be detected indirectly by measurements of B-mode polarization of the CMB, as was attempted by BICEP2. Although BICEP2 interpreted their results as an IGW detection, further analysis proved that some 38% of the polarization detected was due to cosmic dust. It is unclear whether the remaining signal observed by BICEP2 can be interpreted as an IGW detection or as pollution of the CMB signal due to cosmic dust. Further speculation on the nature of BICEP2's readings, evidently, requires greater observation of the multipole moment $\ell \sim 80$ range corresponding to the recombination bump in the B-mode power spectrum.

REFERENCES

[1] Barkats, D. et al. 2005. First Measurements of the Polarization of the Cosmic Microwave Background Radiation at Small Angular Scales from CAPMAP. arxiv.org.

[2] BICEP1 Collaboration. 2015. Degree-Scale CMB Polarization Measurements from Three Years of BICEP1 Data. arxiv.org.

[3] BICEP2 Collaboration. 2014. Detection of *B*-Mode Polarization at Degree Angular Scales by BICEP2. arxiv.org.

[4] BICEP2/Keck and Planck Collaborations. 2015. A Joint Analysis of BICEP2/*Keck Array* and *Planck* Data. arxiv.org.

[5] Bock, J. 2014. Detection of B-mode Polarization at Degree Scales using BICEP2. Presented at: Richard P. Feynman Lecture Hall, California Institute of Technology; Pasadena, CA.

[6] Boyle, Latham A. 2006. Gravitational Waves and the Early Universe [dissertation]. [Princeton, (NJ)]: Princeton University. arxiv.org.

[7] ESA and the Planck Collaboration. 2006. Combined Focal Plane of Planck's Two Instruments. esa.int.

[8] ESA and the Planck Collaboration. 2009. Planck Spacecraft. esa.int.

[9] ESA and the Planck Collaboration. 2012. Planck Instruments in Brief. esa.int.

[10] ESA and the Planck Collaboration. 2013. Planck Reveals an Almost Perfect Universe. esa.int.

[11] ESA and the Planck Collaboration. 2015. Polarised emission from Milky Way dust. esa.int.

[12] Griffiths, David J. 2005. Introduction to Quantum Mechanics. Second Edition. Upper Saddle River, NJ: Pearson Prentice Hall.

[13] Griffiths, David J. 2013. Introduction to Electrodynamics. Fourth Edition. Upper Saddle River, NJ: Pearson Prentice Hall.

[14] Hannay, Shaul. 2002. A comparison of designs of off-axis Gregorian telescopes for mm-wave large focal plane arrays.

[15] Hartle, James B. 2003. Gravity: An Introduction to Einstein's General Relativity. First Edition. San Francisco, CA: Addison Wesley.

[16] Hu, Wayne. Electric and Magnetic Modes. background.uchicago.edu.

[17] Jones, William C. 2002. Polarisation Sensitive Bolometers. California Institute of Technology; Pasadena, CA.

[18] Juvela, M. 2015. Dust emission and scattering in dense interstellar clouds. elsevier.com.

[19] Kamionkowski, Marc, Arthur Kosowsky, Albert Stebbins. 1996. Statistics of Cosmic Microwave Background Polarization. arxiv.org.

[20] Kamionkowski, Marc et al. 1996. A Probe of Primordial Gravity Waves and Vorticity. arxiv.org.

[21] Kinney, William H. 2002. Cosmology, Inflation, and the Physics of Nothing. Columbia University; New York, NY. ned.ipac.caltech.edu.

[22] Kleiner, Reinhold et al. 2004. Superconducting Quantum Interference Devices: State of the Art and Applications. California Institute of Technology; Pasadena, CA.

[23] Kosowsky, Arthur. 1994. Cosmic Microwave Background Polarization. arxiv.org.

[24] Liddle, Andrew R. 1999. An Introduction to Cosmological Inflation. arxiv.org.

[25] McCammon, Dan. 2004. Semiconductor Thermistors. University of Wisconsin, Madison; Madison, WI. arxiv.org.

[26] Migdall, Alan. 2015. Measuring Optical Power with Single-Photon Detectors. nist.gov.

[27] Pedrotti, Frank L., Pedrotti, Leno S., Pedrotti, Leno M. 2007. Introduction to Optics. Third Edition. San Francisco, CA: Addison Wesley.

[28] Planck Collaboration. 2015. *Planck* intermediate results. XXII. Frequency dependence of thermal emission from Galactic dust in intensity and polarization. arxiv.org.

[29] Seljac, Uroš. 1997. Measuring Polarization in the Cosmic Microwave Background. arxiv.org.

[30] Seljak, Uroš, Matias Zaldarriaga. 1997. Signature of Gravity Waves in Polarization of the Microwave Background. arxiv.org.

[31] Siliconix. 1997. An Introduction to FETs. colorado.edu.

[32] Takahashi, Yuki D. 2003. Cosmic Microwave Background Polarization: The Next Key Toward the Origin of the Universe. cosmology.berkely.edu.

[33] Zaldarriaga, Matias, Uroš Seljak. 1997. An All-Sky Analysis of Polarization in the Microwave Background. arxiv.org.